

Bilayered vanadium oxide as the host material for reversible beyond lithium ion intercalation

Mallory Clites, Bryan W. Byles, Ekaterina Pomerantseva*

Department of Materials Science and Engineering, Drexel University, 3141 Chestnut Street, Philadelphia, PA 19104, USA

*Corresponding author: Tel: +1 (215) 571-4612; E-mail: epomeran@coe.drexel.edu

Received: 02 December 2016, Revised: 16 January 2017 and Accepted: 27 January 2017

DOI: 10.5185/amlett.2017.1536

www.vbripress.com/aml

Abstract

Bilayered vanadium oxide has emerged as a high-performance cathode material for beyond lithium ion (BLI) battery systems including Na-ion batteries, Mg-ion batteries, and pseudocapacitors. The major structural feature of bilayered V_2O_5 that makes it attractive for such applications is its large interlayer spacing of ~ 10 - 13 Å. This spacing can be controlled via the interlayer content, which can consist of varying amounts of structural water and/or inorganic ions, resulting in numerous chemical compositions. Further, bilayered V_2O_5 can be synthesized via a number of different methods, resulting in morphologies that include xerogel, aerogel, thin films, and 1-D nanostructures. The interlayer spacing, content, and material morphology can all affect the electrochemical performance of this materials family, and in this review, we discuss the role of each of these factors in the reversible cycling of charge-carrying ions beyond lithium. The different bilayered V_2O_5 synthesis methods and resulting compositions are reviewed, and important structure-property-performance insights into the reversible insertion/ extraction of larger/multivalent ions into the bilayered V_2O_5 structure are highlighted. Copyright © 2017 VBRI Press.

Keywords: Layered materials, beyond lithium ion batteries, intercalation, bilayered vanadium oxide.

Introduction

The growing Internet of Things combined with environmental concerns raise demand for affordable, high-performance electrical energy storage systems. Due to their high energy density, Li-ion batteries currently dominate the market. At the same time, as the number of applications requiring batteries grows, combined with emerging applications requiring larger and greater amounts of batteries (i.e. grid level storage), it becomes obvious that new solutions, utilizing more abundant elements than lithium, are needed. Na-ion and Mg-ion batteries, two electrical energy storage systems that belong to beyond lithium ion (BLI) battery family, are attractive candidates as they operate due to reversible intercalation of more abundant Na^+ and Mg^{2+} ions, respectively. However Na^+ ion is 1.43 times larger than Li^+ ion, and Mg^{2+} ion is doubly charged, which leads to the sluggish diffusion of these ions and deteriorated performance compared to that of Li-ion batteries. In addition, Na-ion and Mg-ion batteries (SIBs and MIBs, respectively) operate at lower voltages than Li-ion batteries, and thus higher capacity cathode materials are necessary to increase the energy density of SIBs and MIBs. Recently, it was shown that transition metal compounds with layered structures and large interlayer spacings, such as carbides, oxides and dichalcogenides, can enable a large number of intercalation sites and well defined two-dimensional pathways for ion diffusion, leading to high performance in BLI systems [1]. Among

these materials, layered transition metal oxides show relatively high working voltages, which make them attractive candidates for application as cathodes in BLI batteries.

Layered α - V_2O_5 , also known as orthorhombic vanadium pentoxide, has been extensively investigated as a cathode material for Li-ion batteries [2]. The high capacity was achieved due to the ability of vanadium to reduce from V^{5+} to V^{3+} , which is accompanied by the transfer of two electrons. However, the interlayer distance in α - V_2O_5 is only ~ 4.4 Å, which was shown to not be sufficient to enable rapid transport of Na^+ ions (Fig. 1a) [3, 4]. The larger Na^+ ion with high ionization potential requires more open diffusion channels for efficient transport. Another allotropic modification of layered vanadium pentoxide, so called bilayered (or δ -) V_2O_5 emerged as a promising material for BLI storage. The two-dimensional bilayered V_2O_5 slabs are separated by a large interlayer spacing of ~ 10 - 13 Å (Fig. 1b), which is more than twice larger than that of orthorhombic V_2O_5 . In addition to creating the large two-dimensional ion diffusion channels, the adjustable interlayer spacing can accommodate volume changes associated with reversible intercalation of larger/multivalent ions.

In this review article, we will discuss recent advances shown by bilayered V_2O_5 in intercalation-based beyond lithium ion systems, including Na-ion and Mg-ion batteries, as well as Na-ion pseudocapacitors. We will also provide background on the structure and methodologies

that are used for the synthesis of the material. Due to the absence of long-range order in these materials and the wide range of compositions arising from varying interlayer content, some ambiguity exists in the understanding of their structure. In this review, we refer to all materials in which V_2O_5 bilayers are separated by the large ($> 9\text{Å}$) interlayer spacing as bilayered vanadium oxide, regardless the details of the bilayer structure, interlayer content, and morphology of the material. At the end, we will outline the scientific directions in the area of energy storage that can be explored within the bilayered V_2O_5 material system.

Structure of bilayered $V_2O_5 \cdot nH_2O$ xerogel

Vanadium pentoxide with the large interlayer spacing was first synthesized in a form of a xerogel with water molecules accommodated between V-O layers, and as such, the chemical formula of the material is often written as $V_2O_5 \cdot nH_2O$. Although the material exhibits lamellar ordering and well-ordered local structure, it is only observed on the nanometer length scale without long-range order. Atomic pair distribution function (PDF) technique was used to investigate the structure of the material and proved to be a powerful tool for structural characterization of crystalline materials with significant intrinsic disorder [5]. Later, the structure of $V_2O_5 \cdot nH_2O$ xerogel was refined using density functional theory (DFT) calculations [6]. It was found that the V-O slabs of the xerogel are built by two layers (bilayers) of flipped V_2O_5 chains consisting of square pyramid VO_5 units with a distance of 2.9Å between the vanadium atoms. The structure of each chain in the bilayer is similar to the structure of a single layer in α - V_2O_5 (Fig. 1), with the exception that vanadyl oxygens (V=O at the tip of the square pyramid) point toward the outside of the bilayer (Fig. 1). Interlayer distances in the range of 8.8 - 13.5Å were reported for bilayered vanadium oxide, depending on the material synthesis method [3, 7].

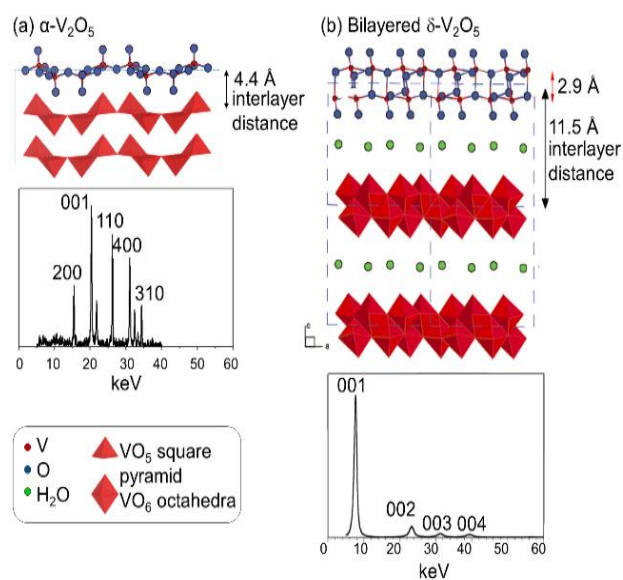
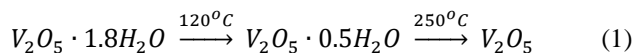


Fig. 1. (a) Crystal structure and XRD pattern of orthorhombic α - V_2O_5 . (b) Crystal structure and XRD pattern of water-containing bilayered δ - V_2O_5 [5].

Water molecules located between the V_2O_5 bilayers are believed to play an important role in stabilizing exceptionally large interlayer distance in $V_2O_5 \cdot nH_2O$ xerogels. Thermogravimetric analysis revealed that there are two types of structural water: (1) water molecules that are located between the bilayers and evaporate from the crystal structure of the xerogel at $\sim 120^\circ\text{C}$ and (2) water molecules that are more strongly bound to V-O layers and leave the structure at $\sim 250^\circ\text{C}$ (Eq. 1).



The amount of the structural water can be precisely determined from the mass loss in the thermogravimetric experiments, and it can vary around 1.8 molecules per V_2O_5 unit, shown in Equation 1, depending on the synthesis conditions. Water content can be further tuned by drying the xerogel at different temperatures below $\sim 300^\circ\text{C}$, the temperature at which bilayered V_2O_5 is believed to become unstable and undergo phase transformation.

Thus, the $V_2O_5 \cdot nH_2O$ xerogel structure is viewed as V_2O_5 bilayers stacked along the c -axis of the unit cell. The stacking sequence is imperfect, leading to the long-range disorder. The unique large, tunable interlayer spacing is believed to be beneficial for the movement of large or multivalent charge-carrying ions in BLI energy storage systems. In addition, structural water can stabilize material structure in multiple cycles of reversible ion intercalation/extraction. It has been shown that structural water molecules can provide electrostatic shielding between intercalating cation and host anions and facilitate diffusion of charge-carrying ions [8, 9].

Synthesis of bilayered vanadium oxide

The $V_2O_5 \cdot nH_2O$ xerogel can be prepared by pouring molten crystalline α - V_2O_5 into deionized water under vigorous stirring and subsequent aging of the formed precipitate for several days [4, 5]. This synthesis approach produces a dark red-brown xerogel film. The dried xerogel forms a fluffy sponge morphology (Fig. 2a) with a large surface area two-dimensional flake structure (Fig. 2b). The flakes are composed of thin nanowires with many nanometer-scaled pores (Fig. 2c). A bilayered vanadium oxide aerogel was synthesized through a sol-gel process by dissolving crystalline α - V_2O_5 in an excess of H_2O_2 . The produced aerogel was aged for 4 days, solvent exchanged with the acetone and dried with supercritical CO_2 at 32°C and 82 bars. The composition of the aerogel was estimated as $V_2O_5 \cdot 1.28H_2O \cdot 0.14C_3H_6O$, and the interlayer distance, determined through XRD analysis, was $\sim 12.4\text{Å}$ [10, 11].

Thin film electrodes of bilayered vanadium oxide were synthesized via electrochemical deposition from aqueous $VOSO_4$ solution. This synthesis approach not only enables control of material thickness on the nanoscale (hence controlling ion diffusion distances), but also creates an intimate, direct contact between the current collector and active electrode material, leading to improved electron transfer. In addition, such electrodes are made without the

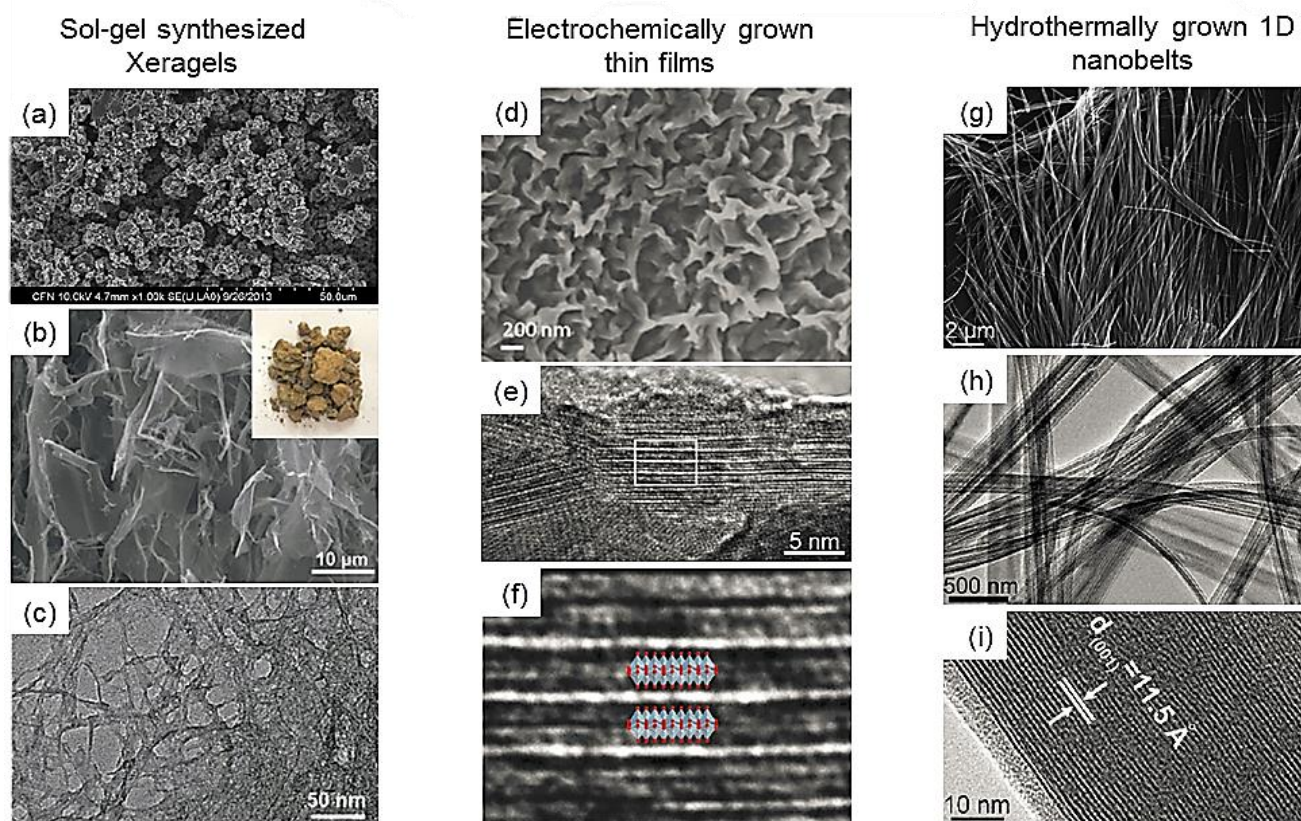


Fig. 2. (a-c) SEM (a [5] and b [4]) and TEM images (c) of sol-gel synthesized xerogels. The inset in (b) shows optical image of synthesized sample [4]. (d-f) Morphologies of electrochemically deposited thin films, with SEM image (d) and TEM images (e and f) shown [3]. (g-i) SEM images (g) and TEM images (h and i) of hydrothermally grown 1D nanostructured morphologies [13].

addition of a conductive additive and polymer binder, minimizing the amount of inactive components in the electrode architecture. The electrodeposited δ - V_2O_5 film consists of nanoribbons with highly porous structure (**Fig. 2d**), which facilitates penetration of the electrolyte and leads to the high electrode/electrolyte contact area. Figures 2e and 2f show the HRTEM images of electrochemically grown δ - V_2O_5 film in conjunction with the lattice model of monoclinic bilayered structure. It was found that the film is composed of interwoven δ - V_2O_5 ribbons. The brightest and thickest line in the images (**Fig. 2e, 2f**) corresponds to the interlayer gap, and the periodicity of the gap ranged from 11.5 to 13.0 Å. Electrodeposition can be used with different conductive substrates with both planar and three-dimensional architectures. The performance of bilayered vanadium electrodes that were electrochemically deposited on stainless steel substrates [12] and nickel foil [3] was investigated in Na-ion cells, while in case of Mg-ion batteries, the film was grown on the surface of porous carbon nanofoam [7]. The high porosity of the carbon nanofoam allowed for increased V_2O_5 loading up to 30 mg/cm².

Bilayered vanadium oxide with a nanobelt morphology can be synthesized using hydrothermal treatment. In this process, VCl_3 is dissolved in a mixture of pyridine and deionized water, followed by heating at 160°C in a Teflon-lined autoclave for 12 hours. The resulting one-dimensional nanobelts (**Fig. 2g, 2h**) have rectangular

cross-sections, with a width of ~90 nm and height of ~50 nm, and are up to few micrometers in length. The nanobelts grow along the [010] direction, and the interlayer distance along the c-axis was found to be 11.5 Å (**Fig. 2i**). These large interlayer channels provide well-defined pathways for facile ion diffusion.

Sodium-ion batteries

The $V_2O_5 \cdot nH_2O$ xerogel cathode exhibited a capacity of 306 mAh g⁻¹ when cycled in a 1.0-4.0 V vs Na/Na⁺ voltage range at a current density of 0.1 A g⁻¹ (**Fig. 3**). This capacity is much higher than that of the α - V_2O_5 xerogel (170 mAh g⁻¹) [4] and corresponds to the intercalation of 2.32 Na⁺ ions per V_2O_5 formula unit. In the second cycle, bilayered vanadium oxide xerogel delivered a capacity of 300 mAh g⁻¹, while the capacity of α - V_2O_5 xerogel dropped to 71 mAh g⁻¹. The coulombic efficiency of the $V_2O_5 \cdot nH_2O$ cathode was ~97.5% in the overall battery testing process, which is much higher than that of the α - V_2O_5 cathode. The $V_2O_5 \cdot nH_2O$ xerogel electrode also demonstrated good rate performance, achieving a capacity of 96 mAh g⁻¹ at an increased current density of 1.0 A g⁻¹, which was attributed to the large interlayer spacing of the bilayered vanadium oxide (**Fig. 3**) [4].

Structural changes of the $V_2O_5 \cdot nH_2O$ xerogel during Na⁺ ion insertion/extraction processes were investigated through ex situ XRD analysis [4]. Drastic shrinkage of the

interlayer spacing, accompanied by a decrease in crystallinity, was observed upon the first intercalation of Na^+ ions. Shrinkage of the interlayer spacing was attributed to a coordination reaction between Na^+ ions and V_2O_5 bilayers. The following extraction of Na^+ ions was found to partially restore both the large interlayer spacing and higher crystallinity of the starting material. However, the initial interlayer spacing was not fully recovered, and this pattern continued with cycling. The collapsing of the layered structure was believed to be a major reason for the capacity fading ($\sim 190 \text{ mAh g}^{-1}$ after 30 cycles at 0.1 A g^{-1}) [4].

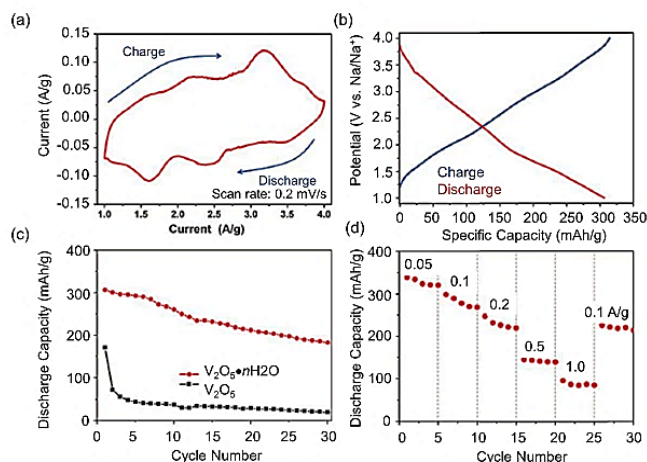


Fig. 3. Electrochemical performance of $\text{V}_2\text{O}_5 \cdot n\text{H}_2\text{O}$ cathodes in Na-ion half cells. (a) Cyclic voltammetry between 1.0-4.0 V at a sweep rate of 0.2 mV s^{-1} . (b) Galvanostatic charge/discharge curves between 1.0-4.0 V at a current density of 0.1 A g^{-1} . (c) Life cycle performance of $\alpha\text{-V}_2\text{O}_5$ and $\text{V}_2\text{O}_5 \cdot n\text{H}_2\text{O}$ cathodes. (d) Rate capabilities of $\text{V}_2\text{O}_5 \cdot n\text{H}_2\text{O}$ cathodes at increasing current densities from 0.05-1.0 A g^{-1} [4].

Amorphous V_2O_5 aerogel was explored as both a cathode [10] and anode [11] material in Na-ion batteries. Cycling of the material in the wide 0.1-4.0 V vs Na/Na^+ voltage range at 14.7 mA g^{-1} demonstrated the high first discharge capacity of 500 mAh g^{-1} , corresponding to the insertion of $\sim 3.4 \text{ Na}^+$ ions per unit formula. Based on the sloping discharge potential profiles, the authors have attributed such high capacity to an intercalation process [11]. This is contrary to the previously suggested conversion reaction at low voltages ($< 1.0 \text{ V}$) leading to the formation of VO and Li_2O [14, 15].

When the upper voltage limit was decreased to 2.0 V vs Na/Na^+ (with the lower voltage limit remaining the same at 0.1 V vs Na/Na^+), a capacity of 250 mAh g^{-1} was observed on the first charge cycle, and the discharge capacity remained slightly over 200 mAh g^{-1} in the subsequent 20 cycles [11]. At higher current rates of 1C and 2C in this voltage range, capacities of 125 mAh g^{-1} and 71 mAh g^{-1} were observed, respectively, indicating decent rate capability. Additionally, the cycling stability of the V_2O_5 aerogel was tested at a current density of 100 mA g^{-1} between 0.01-1.5 V vs Na/Na^+ to more closely meet voltage range requirements for anode materials. The initial capacity of $\sim 200 \text{ mAh g}^{-1}$ dropped to 146 mAh g^{-1} after 40 cycles. The fast capacity fading was explained by the

possibility of a secondary charge storage mechanism different from intercalation. The high initial performance parameters in the 0.01-1.5 V vs Na/Na^+ voltage range were attributed to the large interlayer spacing and short diffusion paths characteristic of the aerogel morphology [11].

To test the material as a cathode, amorphous V_2O_5 aerogel was galvanostatically cycled between 1.5-4.0 V vs Na/Na^+ at 56 mA g^{-1} , delivering a modest capacity of 150 mAh g^{-1} [10]. Upon increasing the current density to 560 mA g^{-1} , the electrode delivered slightly more than 50% of its initial capacity, indicating that a more ordered bilayered vanadium oxide structure is needed to achieve high performance in a voltage range typical for cathode materials.

Cycling performance of the electrochemically grown bilayered vanadium oxide in Na-ion cells was compared to that of orthorhombic $\alpha\text{-V}_2\text{O}_5$ [3]. The latter was obtained by annealing electrochemically grown $\delta\text{-V}_2\text{O}_5$ film in oxygen atmosphere at 500°C , which ensured the same film thickness and intimate contact with the current collector for both materials, thus making the crystal structure of the films the only difference affecting their performance.

Although both materials exhibited a capacity of $\sim 230\text{-}250 \text{ mAh g}^{-1}$ when cycled in the 1.5-3.8 V voltage range at 20 mA g^{-1} (Fig. 4a), the bilayered V_2O_5 demonstrated better electrochemical stability, maintaining a capacity of 250 mAh g^{-1} during the first four cycles while the capacity of the $\alpha\text{-V}_2\text{O}_5$ dropped to $\sim 150 \text{ mAh g}^{-1}$ after four cycles (Fig. 4a). The initial, higher voltage part of the first discharge curve of $\delta\text{-V}_2\text{O}_5$ electrode shows a smooth slope which corresponds to the capacity of $\sim 235 \text{ mAh g}^{-1}$. Such shape of the voltage profile is indicative of solid solution intercalation mechanism. The shorter steep part of the discharge curve (lower voltage section), contributing $\sim 15 \text{ mAh g}^{-1}$, was attributed to a capacitive mechanism of charge storage.

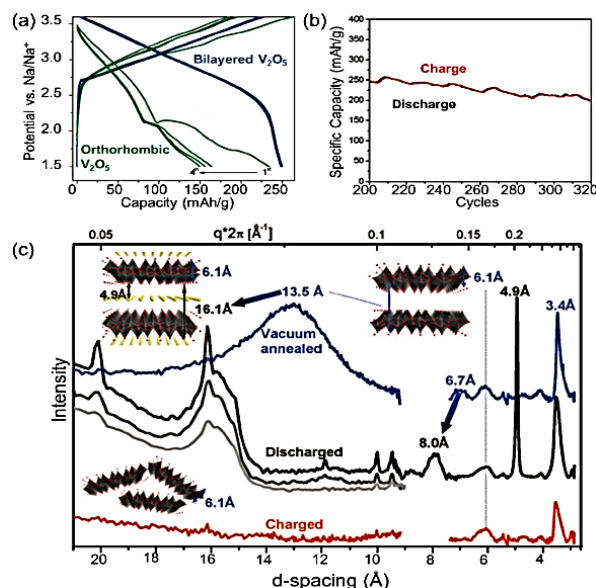


Fig. 4. Electrochemical performance of $\delta\text{-V}_2\text{O}_5$ cathodes in Na-ion half cells using 1M NaClO_4 in PC. (a) Galvanostatic charge/discharge curves between 1.5-3.8 V at a current density of 20 mA g^{-1} . (b) Life cycle performance from cycles 200-320. (c) Change in XRD patterns of $\delta\text{-V}_2\text{O}_5$ cathodes upon charging and discharging [3].

Bilayered vanadium oxide electrodes have also demonstrated high stability over extended cycling (350 cycles) at different current densities. The electrodes were cycled at 20 mA g⁻¹ for the first 30 cycles, followed by 170 cycles at higher current densities ranging from 60 to 630 mA g⁻¹, and then finally at 20 mA g⁻¹ for 120 cycles. In the final 120 cycles, the electrodes still achieved 85% of their initial capacities (Fig. 4b). It is believed that the large interlayer spacing of the bilayered structure is crucial for efficiency and stability of the bilayered vanadium oxide electrode in Na-ion batteries. At the same time, the electrode architecture that combined an excellent interface between current collector and active battery material with high exposed surface area was also indicated as an important attribute for achieving the high rate and cycling performance demonstrated by electrochemically grown bilayered V₂O₅ film electrodes [3].

In-situ, Small- and Wide-Angle X-ray scattering (SAXS and WAXS) techniques were used to gain an understanding of the charge storage mechanism of the electrochemically grown bilayered vanadium oxide by investigating changes in the structure of the material upon sodium intercalation and extraction. It was found that upon initial discharge, the interlayer spacing changes from 13.5 Å to 16.1 Å. The features in the SAXS and WAXS spectra (Fig. 4c) indicate that improved stacking order is induced by Na⁺ ion intercalation. Extraction of Na⁺ ions on charge removes this stacking order [3]. The crystallinity of the material was not affected by sodium cycling even after 80 discharge/charge cycles. These results contradict shrinkage of the interlayer spacing and amorphization of the active electrode material reported for the V₂O₅·nH₂O xerogel [4], indicating an importance of the material synthesis approach for obtaining electrodes with high electrochemical performance.

In another report, bilayered V₂O₅ nanobelts delivered a capacity of ~206 mAh g⁻¹ when cycled in Na-ion cells between 1.0-4.0 V vs Na/Na⁺ at 80 mAh g⁻¹ [16]. The capacity increased on the second and third cycle to 231 and 223 mAh g⁻¹, respectively.

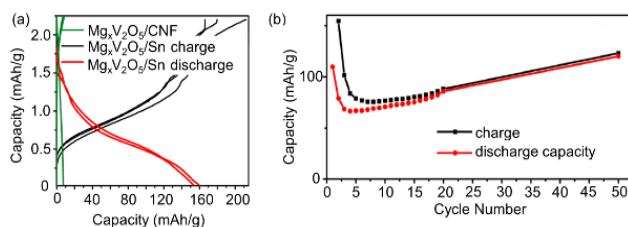


Fig. 5. Electrochemical performance of δ -V₂O₅ cathodes in Mg-ion half cells. (a) Galvanostatic charge/discharge curves between 1.5-3.8 V at a current density of 20 mA g⁻¹. (b) Life cycle performance from cycles 1-50 [7].

It was suggested that the electrolyte diffused into interlayer space of δ -V₂O₅ in the first cycle and facilitated electrochemical reaction on following cycles, leading to increased capacities [16]. The electrode exhibited a discharge capacity of 170 mAh g⁻¹ after 100 cycles, demonstrating

relatively stable cycling performance. The rate capability evaluation revealed that the bilayered vanadium oxide nanobelts maintained a capacity of 134 mAh g⁻¹ when the current density was increased to 640 mA g⁻¹. The superior electrochemical performance of δ -V₂O₅ nanobelts was ascribed to the large interlayer spacing in the material and orientation of the interlayer channels perpendicular to the exposed (100) nanobelt facets providing easy access to Na⁺ ions from electrolyte. The small thickness of the nanobelts (~50 nm) also provides a short distance for Na⁺ ion to diffuse, thus leading to the improved kinetics of the discharge/charge processes [16].

Magnesium-ion batteries

The structural evolution of the V₂O₅·nH₂O xerogel in reversible Mg²⁺ ion intercalation processes was investigated using a combination of X-ray scattering, spectroscopic, computational, and electrochemical methods [17]. The xerogel electrode was cycled against Mg metal disk using 1 M Mg(TFSI)₂ in diglyme as an electrolyte. When cycled between 0.0-3.2 V vs Mg/Mg²⁺ at a current density of 20 μ A/cm², the bilayered V₂O₅·nH₂O electrode delivered a first discharge capacity of ~50 mAh g⁻¹, which corresponds to the intercalation of 0.25 mol of Mg per mole of V₂O₅. Small and gradual capacity escalation was observed over the 10 initial cycles, and this was attributed to the penetration of the electrolyte into the interlayer space and increase in the microscopic reaction area [17].

Electrochemical evidence at higher currents revealed that the electrochemical insertion of Mg²⁺ ions into the xerogel structure is a slow kinetic process. The structural water within the material was found to be stably bound to the vanadium oxide structure and did not leave the cathode material and dissolve in the electrolyte during cycling. The initial large interlayer spacing of the V₂O₅·nH₂O xerogel (12.8 Å) contracts upon Mg²⁺ ion intercalation (discharge) to 10.9 Å, and it expands back to the original value for the fully charged electrode. Solid-state nuclear magnetic resonance spectroscopy revealed that magnesium is octahedrally coordinated and confirmed co-intercalation of the electrolyte solvent for the first time. Despite the relatively low capacities demonstrated in this work, the detailed material characterization shed light upon the Mg²⁺ ion intercalation mechanism in a bilayered V₂O₅·nH₂O xerogel [17].

Separately, a high surface area bilayered vanadium oxide film, which was electrodeposited on carbon nanofoam and electrochemically preintercalated with magnesium, was cycled against a Sn anode in Mg-ion cells with 1M Mg(ClO₄)₂ in acetonitrile as the electrolyte [7]. This cell delivered reversible capacity of 150 mAh g⁻¹ when cycled between 0.0-2.2 V vs Mg/Mg²⁺ at 20 mA g⁻¹ (Fig. 5a). Using MD simulations, it was shown that the presence of structural water and ensuring hydration of the intercalated Mg²⁺ ions are necessary for reversible cycling [7]. The detailed structural investigation revealed that upon magnesium intercalation the interlayer spacing decreases from 13.1 Å to 11.0 Å and Mg²⁺ ions are

localized near terminal hydroxyl groups in the interlayer space of the bilayered V_2O_5 . This behavior is very different from the interlayer changes observed during sodiation of electrochemically grown δ - V_2O_5 , where the interlayer spacing increased to accommodate for the intercalation of the relatively large Na^+ ions [3]. In addition to the nearing of V_2O_5 bilayers due to the strong interactions between doubly charged magnesium ions and terminal hydroxyl groups, Mg-intercalated bilayered V_2O_5 exhibits better structural ordering. However, upon extended cycling for 50 cycles, the bilayered vanadium oxide structure becomes more disordered and polycrystalline, although specific capacity continually increases (Fig. 5b) [7].

Using first-principles calculations the effect of water on the voltage exhibited by the stable phases of Mg - $V_2O_5 \cdot nH_2O$ xerogel was investigated [8]. It was found that Mg^{2+} ions in the interlayer space of the bilayered vanadium oxide are coordinated by two lattice oxygens and four oxygen atoms from interlayer water molecules. The voltage of Mg^{2+} ions intercalation was computed in cases of wet, dry, and super dry electrolytes, and water from the electrolyte was allowed to co-intercalate together with Mg^{2+} ions. For low magnesium concentration, the voltage linearly decreases from 2.9 to 2.46 V vs Mg/Mg^{2+} when water content was changed from wet to dry conditions, and it remained stable at 2.46 V vs Mg/Mg^{2+} in a super dry electrolyte. For high magnesium concentration, the voltage decreased from 2.55 V to 2.45 V vs Mg/Mg^{2+} in wet electrolyte, it remained stable at \sim 2.45 V vs Mg/Mg^{2+} in a dry electrolyte, and the voltage slightly grew up to 2.46 V vs Mg/Mg^{2+} in a super dry electrolyte [8]. Therefore, given the wide diversity of the synthesis methods for the preparation of bilayered vanadium oxide that allow for the tuning of the structural water content in the interlayer

spacing, this material can serve as a unique platform for the investigation of the role of structural water in BLI storage electrodes.

Pseudocapacitors

Capacitive energy storage, which includes double-layer capacitors (also known as supercapacitors or ultracapacitors) and pseudocapacitors, attracts attention due to the faster kinetics of the charge and discharge processes, leading to shorter charging times and higher power densities than those reported for batteries. In addition, capacitive storage offers long-term electrode stability resulting in longer cycle life than that of batteries.

Pseudocapacitive materials emerged as an electrochemical system that can enable increased energy density due to a faradaic charge storage mechanism that involves redox reactions, in contrast to supercapacitors, which operate due to surface-based charge storage. Pseudocapacitors can utilize either aqueous or non-aqueous electrolytes, depending on the electrode materials, and many different charge-carrying ions. Abundant charge-carrying ions, such as Na^+ ions, are of particular interest for the development of low-cost pseudocapacitors.

As discussed above, the large interlayer spacing of the bilayered vanadium oxide, combined with the phase stability during cycling, is attractive for the pseudocapacitive application of this material due to the increased ion diffusion which was shown even for the large Na^+ ions [3, 4, 16]. However, like most oxides, δ - V_2O_5 has relatively low electronic conductivity ($\sigma \sim 10^{-6}$ to $1 \Omega^{-1} \cdot cm^{-1}$ [18]), which needs to be improved to explore this material as pseudocapacitive electrode.

A smart electrode architecture has been realized by integrating bilayered V_2O_5 nanowires with highly

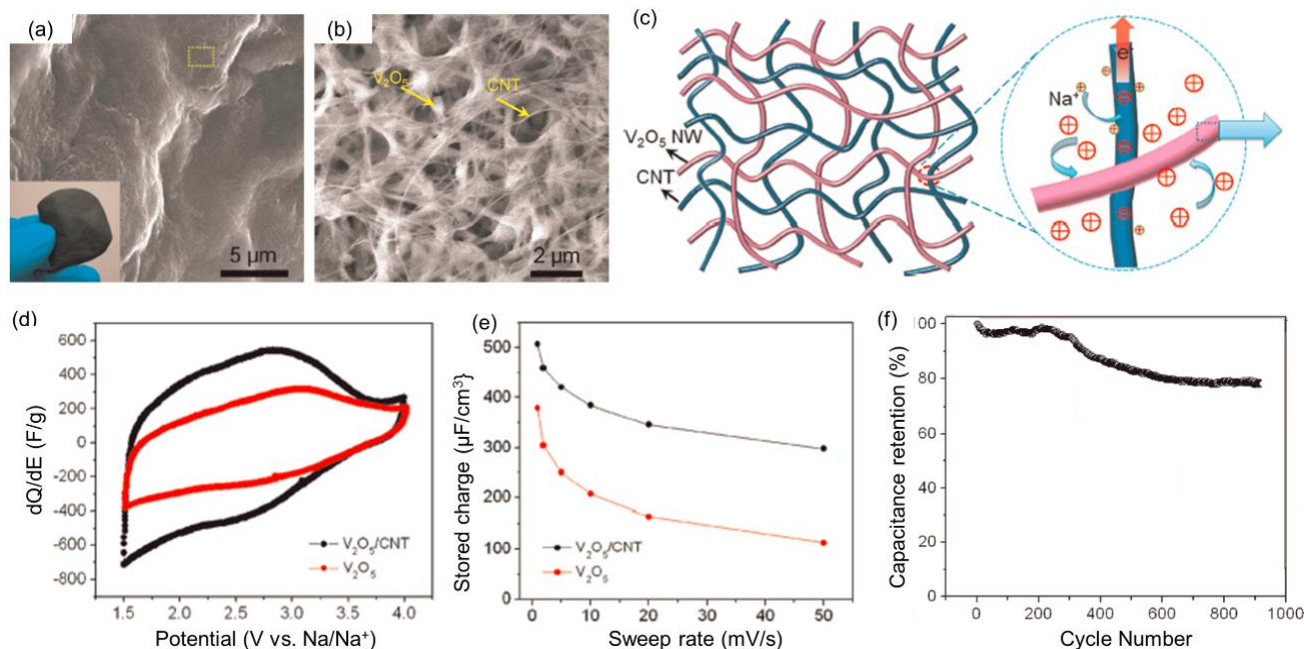


Fig. 6. (a and b) SEM images of flexible V_2O_5/CNT composite films. The inset in (a) shows an optical image of the flexible thin film. (c) Schematic representation of V_2O_5/CNT composite. (d) Cyclic voltammograms of V_2O_5 and V_2O_5/CNT films from 1.0-4.0 V at a scan rate $2 mV \cdot s^{-1}$ in 1 M $NaClO_4$ in two electrode cells. (e) Stored charge versus sweep rate for V_2O_5 and V_2O_5/CNT films. (f) Cycle life performance for 900 cycles at a C-rate of 60C [13].

conductive carbon nanotubes (CNTs). The electrode was prepared by a one-pot hydrothermal treatment of aqueous vanadium oxide precursors containing modified hydrophilic CNTs [13]. The product of the hydrothermal process was filtered and washed, forming a free-standing, flexible film (Fig. 6a). The porous composite electrode architecture consisted of the interpenetrating networks of V_2O_5 nanowires and CNTs (Fig. 6b). Such porous structure can be easily filled with the electrolyte resulting in a large contact area between the active material (δ - V_2O_5) and electrolyte (1M $NaClO_4$ in a propylene carbonate solution) and hence improved access of charge-carrying ions (Na^+ ions) to the active material surfaces for intercalation. The continuous conductive CNT network enables effective electron transport, while the small diameter of the δ - V_2O_5 nanowires offers short ion diffusion distances (Fig. 6c). Thermogravimetric analysis showed that the nanocomposite contained 13 wt. % of CNTs, a similar amount of conductive additive to what is found in commercial battery electrodes. This V_2O_5 /CNT composite architecture provides facile sodium intercalation/deintercalation and fast electron transfer, thus meeting the requirements for high-performance pseudocapacitive electrodes [13].

The V_2O_5 /CNT electrode delivered a capacity of ~ 400 $C\ g^{-1}$ when cycled between 1.5-3.5 V, which is significantly higher than that of a pure V_2O_5 nanowire electrode (~ 300 $C\ g^{-1}$) (Fig. 6d). The rate capability experiments (Fig. 6e) showed that nanocomposite electrode exhibited much higher capacities, compared to the pure V_2O_5 electrode, at increased sweep rates. This result indicates the improved kinetics of the discharge and charge processes in the V_2O_5 /CNT composite electrode. Moreover, the nanocomposite retained $\sim 80\%$ of the initial capacity after 900 cycles at a rate of 60 C (Fig. 6f) [13].

Overall, electrochemical testing of the V_2O_5 /CNT electrode in Na-ion cells confirmed that the nanocomposite demonstrated much better rate capability and charge storage compared to the pure V_2O_5 electrode. Such high performance was ascribed to both the structure of the redox active electrode component, δ - V_2O_5 , providing a large interlayer spacing for Na^+ ion intercalation and the electrode architecture providing enhanced electrolyte access and high electronic conductivity through the continuous CNT network [13].

Chemical pre-intercalation approach

A modified sol-gel synthesis strategy can be used to chemically pre-intercalate inorganic ions into the structure of bilayered vanadium oxide. Both charge-carrying ions (Na^+ ions in cases of Na-ion batteries [19] and Mg^{2+} ions in case of Mg-ion batteries [20, 21]) and electrochemically inactive ions (such as iron in case of Na-ion batteries [22]) were chemically inserted between the δ - V_2O_5 bilayers. This pre-intercalation was accomplished through the addition of ion precursors into the reaction mixture during the sol-gel process, resulting the trapping of ions in the interlayer space of bilayered vanadium oxide during precipitate formation.

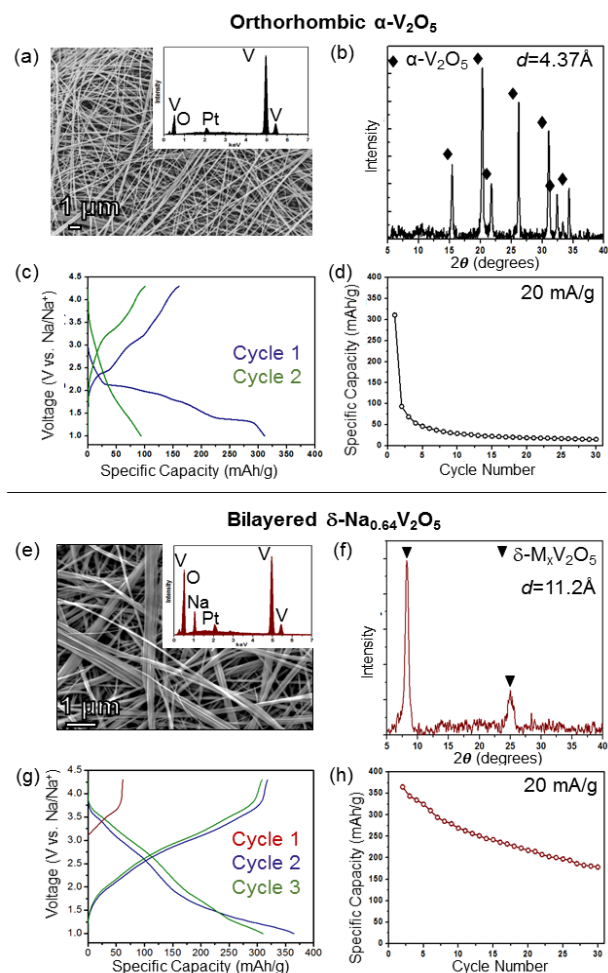


Fig. 7. Comparison of orthorhombic and bilayered δ - $Na_xV_2O_5$ phased materials. (a, e) SEM images of both samples with EDX insets. (b, f) XRD patterns labeled with interlayer spacings, calculated from the (001) peak position for each phase. (c, g) Galvanostatic discharge/charge curves in Na-ion half cells from 1.0-4.3 V at a current density of 20 $mA\ g^{-1}$. (d, h) Life cycle performance for 30 cycles in Na-ion half cells at 20 $mA\ g^{-1}$.

A Na-containing bilayered vanadium oxide was obtained by dissolving NaCl in an aqueous 15 wt. % H_2O_2 solution followed by the addition of α - V_2O_5 powder. The precipitate was aged for 4 days to allow for the formation of bilayers [23]. To maximize sodium content in the material, the aged precipitate was hydrothermally treated in 5M NaCl at 220°C for 24 hours [19]. Interestingly, when NaCl was not added during the sol-gel or hydrothermal treatment step of the material synthesis, nanowires of the orthorhombic α - V_2O_5 formed (Fig. 7, a-b). The Na-containing V_2O_5 also had a nanowire morphology with the Na:V ratio of 0.36, but it crystallized in a bilayered phase (Fig. 7, e-f). The interlayer distance in the δ - $Na_{0.72}V_2O_5$ bilayered nanowires is ~ 11.2 Å. While both α - V_2O_5 and δ - $Na_{0.72}V_2O_5$ samples have nanowire morphologies, they show distinctly different behavior in the electrochemical Na^+ ion cycling. α - V_2O_5 exhibited an initial capacity of ~ 310 $mAh\ g^{-1}$, which quickly faded to ~ 30 $mAh\ g^{-1}$ after only 10 cycles (Fig. 7, c-d). At the same time, the δ - $Na_xV_2O_5$ phase not only showed a higher initial capacity of ~ 365 $mAh\ g^{-1}$, but the capacity also decreased much slower, with a capacity of >250 $mAh\ g^{-1}$ after 10 cycles and ~ 150 $mAh\ g^{-1}$ after 50

cycles (**Fig. 7, g-h**). These results were attributed to the large interlayer spacing of the chemically preintercalated bilayered vanadium oxide, which provided a large number of sites for Na^+ ion intercalation and facilitated Na^+ ion diffusion [19].

A Mg-preintercalated vanadium oxide xerogel with a bilayered crystal structure was prepared by dissolving MgV_2O_6 in water and then treating with an ion exchange resin to form a magnesium deficient $\text{Mg}_x\text{V}_2\text{O}_5$ phase [20, 21] with the interlayer spacing of 12.3 Å [20]. Inductively coupled plasma-optical emission spectroscopy and thermogravimetric analysis revealed that the chemical formula of the obtained material can be written as $\text{Mg}_{0.1}\text{V}_2\text{O}_5 \cdot 1.8\text{H}_2\text{O}$ [20]. Evaluation of the electrochemical performance of this material in Mg-ion cells showed that it delivered capacity $>250 \text{ mAh g}^{-1}$ under C/10 discharge over seven cycles. Such capacity corresponds to the intercalation of one equivalent of Mg^{2+} ions per formula unit of vanadium oxide [20]. Further, the following report from the same group demonstrated that both magnesium and water content can be tuned through the sol-gel based synthesis approach [21]. Two phases with the composition of $\text{Mg}_{0.1}\text{V}_2\text{O}_5 \cdot 2.35\text{H}_2\text{O}$ and $\text{Mg}_{0.2}\text{V}_2\text{O}_5 \cdot 2.46\text{H}_2\text{O}$ were prepared. Both phases had similar interlayer spacing of 14.3 Å. $\text{Mg}_{0.1}\text{V}_2\text{O}_5 \cdot 2.35\text{H}_2\text{O}$ yielded high discharge capacity of 140 mAh g^{-1} with near 100% efficiency, high voltage of 3.0 V (vs Mg^{2+}/Mg), and high energy density of 420 mWh g^{-1} , thus demonstrating promise for application as a cathode in Mg-ion batteries (**Fig. 8**) [21].

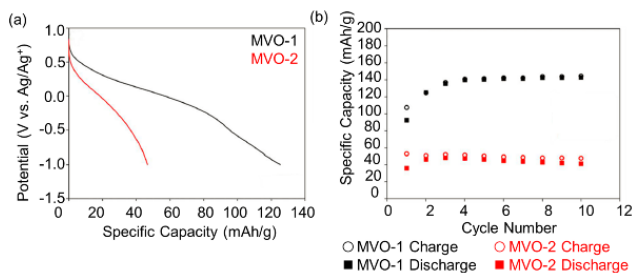


Fig. 8. Electrochemical performance of $\delta\text{-Mg}_x\text{V}_2\text{O}_5 \cdot n\text{H}_2\text{O}$ cathodes in three electrode Mg-ion cells. (a) Galvanostatic discharge profiles for $\delta\text{-Mg}_x\text{V}_2\text{O}_5 \cdot n\text{H}_2\text{O}$ cathodes in Mg-ion cells from -1.0-0.85 V. (b) Initial capacity retention of $\delta\text{-Mg}_x\text{V}_2\text{O}_5 \cdot n\text{H}_2\text{O}$ cathodes [20].

Chemical insertion of iron ions was achieved by using iron (III) acetylacetonate and V_2O_5 sol as precursors that were hydrothermally treated at 180°C for 48 hours [23]. The interlayer spacing in the formed Fe-VO_x was calculated to be $\sim 10.6 \text{ \AA}$. Interestingly, material synthesized using the same approach but without addition of iron precursor formed vanadium oxide with a bilayered crystal structure containing a larger interlayer spacing of 14.0 \AA . This result supports the unique ability to control large interlayer spacing of bilayered vanadium oxide by tuning its interlayer content. It was established that pre-intercalation of iron ions substantially reduces the change of the interlayer spacing caused by reversible large Na^+ ion intercalation and extraction (**Fig. 9a**). While Fe-free bilayered vanadium oxide electrode showed change in the

lattice c parameter of 3.74 \AA , a change of only 0.49 \AA was measured in case of Fe-VO_x . As the result of such iron ion stabilization effect, Fe-containing vanadium oxide exhibited enhanced cycling and rate performance [22]. Fe-VO_x materials yielded higher discharge capacities of 184 mAh g^{-1} compared to the VO_x sols which only demonstrated 161 mAh g^{-1} (**Fig. 9b**). In addition, the inclusion of iron into the interlayer spacing of the bilayered phase also led to increased capacity retention at increased current rates, with Fe-VO_x materials demonstrating 92 mAh g^{-1} at 1C compared to only 43 for VO_x counterparts (**Fig. 9c**) [22].

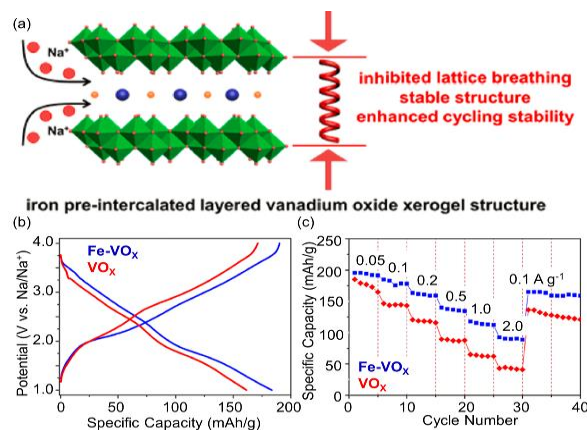


Fig. 9. (a) Schematic representation of ion-stabilization technique that can be used to inhibit lattice breathing upon Na^+ ion insertion and extraction. (b) Galvanostatic discharge/charge curves of V_2O_5 and $\text{Fe}_x\text{V}_2\text{O}_5$ materials from 1.0-4.0 V at a current density of 0.1 A g^{-1} in Na-ion half cells [19].

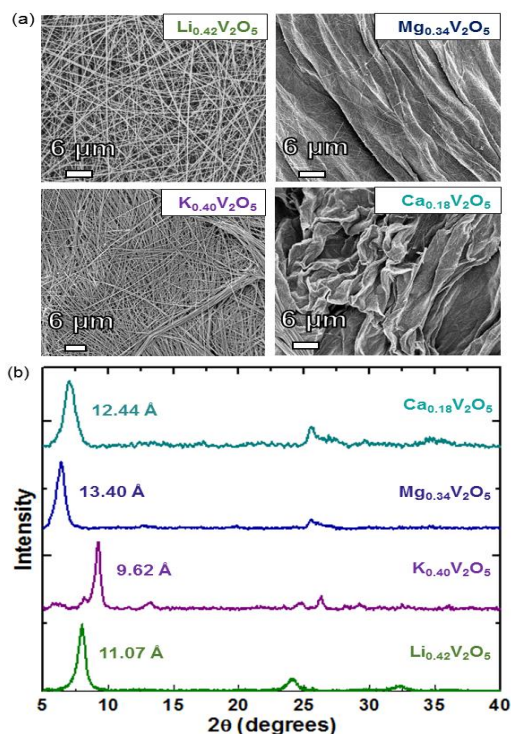


Fig. 10. (a) SEM morphologies of Li-, K-, Mg-, and Ca-intercalated materials and (b) corresponding XRD patterns from $5\text{-}40^\circ 2\theta$. Interlayer spacing for each sample has been labeled by the (001) peak from which it was calculated.

Interestingly, we found that the large interlayer distance can be chemically controlled by changing the nature of the preintercalated ion, with the interlayer spacing ranging from 9.62 Å to 13.40 Å in δ - $M_xV_2O_5$ ($M = \text{Li, Na, K, Mg, and Ca}$), (Fig. 10) [24]. We would like to emphasize that this is the first time that chemical pre-intercalation of doubly charged ions into the structure of vanadium oxide was achieved. Ion intercalation into layered materials with large interlayer spacings can be used as a strategy to stabilize these materials during electrochemical cycling and is currently investigated in our laboratory.

Conclusion and future perspectives

Bilayered vanadium oxide demonstrated advanced electrochemical performance as an electrode material in both Na-ion and Mg-ion batteries, which was attributed to the large (10 – 13 Å) interlayer spacing separating V_2O_5 bilayers and forming open two-dimensional channels for ion diffusion. The interlayer spacing was shown to be defined by the nature and amount of the interlayer species – structural water and inorganic ions. Within the achieved range of the interlayer distance values, materials with the largest spacing often show the highest electrochemical performance. Therefore, it will be important to develop synthesis approaches that would allow for expansion of the layers further and, possibly, produce single-layer vanadium oxide nanoflakes, similarly to the exfoliation of two-dimensional materials such as transition metal dichalcogenides (TMDCs) and transition metal carbides and carbonitrides (MXenes) [25, 26]. If successful, bilayered vanadium oxide with the largely expanded layers (> 13 Å) has the potential to not only exhibit even greater performance in SIBs and MIBs, but also show high electrochemical activity in other intercalation-based BLI systems, such as K-ion and Al-ion batteries.

The ability to control the amount of structural water in the bilayered crystal structure opens a unique opportunity to understand the role of water in BLI electrochemical systems. Recent reports suggest that water molecules can stabilize a material's structure, leading to better capacity retention, and facilitate ions diffusion, leading to higher capacities and faster charge/discharge processes. However, in some cases, water-containing δ - V_2O_5 still shows moderate performance. These observations raise questions, such as (1) is there an optimal amount of the structural water that enables highest performance? and (2) does localization and the form of water (water molecules, hydroxyl groups, or hydronium ions) play a role in the performance? Answers to these questions could be obtained using bilayered vanadium oxide as a model system.

Further, despite the promising electrochemical properties of bilayered V_2O_5 , the mechanism of charge storage in this material in BLI systems is not well understood. The mechanism, which can differ depending on the interlayer spacing and interlayer content, can include elements of three well-known processes: bulk intercalation, intercalation pseudocapacitance, and surface storage. Elucidating the mechanism of larger/multivalent

ion storage in the bilayered vanadium oxide can provide valuable insight into the behavior of other 2D materials (TMDCs and MXenes) in BLI electrochemical intercalation processes.

The excellent performance of the electrochemically grown bilayered V_2O_5 in both Na-ion and Mg-ion batteries highlights the importance of the intimate interface between poorly conductive oxide and a current collector material. Therefore, we believe that close attention should be paid in the future to creating composite architectures integrating bilayered vanadium oxide and nanostructured carbon materials. The targeted architectures should meet the following requirements: (1) continuous porous conductive network built by a carbon component, (2) small thickness of the bilayered V_2O_5 on the surface of carbon enabling short ion diffusion distances, and (3) intimate, stable, face-to-face interface between carbon and vanadium oxide. Due to the ability to synthesize bilayered V_2O_5 through sol-gel process, in which solid material is produced from chemically homogeneous solutions, such composite architectures can be fabricated by introducing the carbon component into the sol-gel reaction mixture. In this case, vanadium oxide bilayers are likely to grow on carbon surfaces, producing the structure that meets aforementioned requirements. These composite electrodes have the potential to demonstrate record high performance enabled by rapid ion and electron transport. Thus, through careful tailoring of electrode architectures, interlayer spacing, and interlayer content, bilayered V_2O_5 can not only be used as a model system gain information on fundamental mechanisms of charge storage in BLI systems, but also for use as high performing electrodes in future BLI batteries.

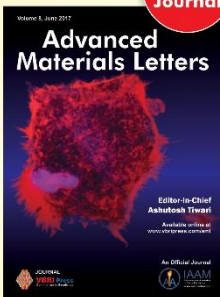
Acknowledgements

The authors acknowledge the startup funding from Drexel University.


References

1. Peng, L.; Zhu, Y.; Chen, D.; Ruoff, R. S.; Yu, G.; *Adv. Energy Mat.*, **2016**, *6*, 11.
DOI: [10.1002/aenm.201600025](https://doi.org/10.1002/aenm.201600025)
2. Whittingham, M. S.; *Chem.Reviews.*, **2004**, *104*, 10.
DOI: [10.1021/cr020731c](https://doi.org/10.1021/cr020731c)
3. Tepavcevic, S.; Xiong, H.; Stamenkovic, V. R.; Zuo, X.; Balasubramanian, M.; Prakapenka, V. B.; Johnson, C. S.; Rajh, T.; *ACS Nano*, **2012**, *6*, 1.
DOI: [10.1021/nn203869a](https://doi.org/10.1021/nn203869a)
4. Wei, Q.; Liu, J.; Feng, W.; Sheng, J.; Tian, X.; He, L.; An, Q.; Mai, L.; *J. of Mat. Chem. A*, **2015**, *3*.
DOI: [10.1039/c5ta00502g](https://doi.org/10.1039/c5ta00502g)
5. Petkov, V.; Trikalitis, P. N.; Bozin, E. S.; Billinge, S. J. L.; Vogt, T.; Kanatzidis, M. G.; *JACS*, **2002**, *124*, 34.
DOI: [10.1039/c5ta00502g](https://doi.org/10.1039/c5ta00502g)
6. Kristoffersen, H. H.; Metiu, H.; *J. of Phys. Chem. C*, **2016**, *120*, 7.
DOI: [10.1021/acs.jpcc.5b12418](https://doi.org/10.1021/acs.jpcc.5b12418)
7. Tepavcevic, S.; Liu, Y.; Zhou, D.; Lai, B.; Maser, J.; Zuo, X.; Chan, H.; Král, P.; Johnson, C. S.; Stamenkovic, V.; Markovic, N. M.; Rajh, T.; *ACS Nano*, **2015**, *9*, 8.
DOI: [10.1021/acs.nano.5b02450](https://doi.org/10.1021/acs.nano.5b02450)
8. Sai Gautam, G.; Canepa, P.; Richards, W. D.; Malik, R.; Ceder, G.; *Nano Letters*, **2016**, *16*, 4.
DOI: [10.1021/acs.nanolett.5b05273](https://doi.org/10.1021/acs.nanolett.5b05273)
9. Wang, R. Y.; Shyam, B.; Stone, K. H.; Weker, J. N.; Pasta, M.; Lee, H.-W.; Toney, M. F.; Cui, Y.; *Adv. Energy Mat.*, **2015**, *5*, 12.
DOI: [10.1002/aenm.201401869](https://doi.org/10.1002/aenm.201401869)

10. Moretti, A.; Maroni, F.; Osada, I.; Nobili, F.; Passerini, S.; *ChemElectroChem*, **2015**, 2, 4.
DOI: [10.1002/celec.201402394](https://doi.org/10.1002/celec.201402394)
11. Moretti, A.; Secchiaroli, M.; Buchholz, D.; Giuli, G.; Marassi, R.; Passerini, S.; *J. Electrochem. Soc.*, **2015**, 162, 14.
DOI: [10.1149/2.0711514jes](https://doi.org/10.1149/2.0711514jes)
12. Li, H.-Y.; Yang, C.-H.; Tseng, C.-M.; Lee, S.-W.; Yang, C.-C.; Wu, T.-Y.; Chang, J.-K.; *J. of Power Sources*, **2015**, 285.
DOI: [10.1016/j.jpowsour.2015.03.086](https://doi.org/10.1016/j.jpowsour.2015.03.086)
13. Chen, Z.; Augustyn, V.; Jia, X.; Xiao, Q.; Dunn, B.; Lu, Y.; *ACS Nano*, **2012**, 6, 5.
DOI: [10.1021/nm300920e](https://doi.org/10.1021/nm300920e)
14. Augustyn, V.; Dunn, B.; *Electrochimica Acta*, **2013**, 88.
DOI: [10.1016/j.electacta.2012.10.145](https://doi.org/10.1016/j.electacta.2012.10.145)
15. Almeida, E. C.; Abbate, M.; Rosolen, J. M.; *Solid State Ionics*, **2001**, 140, 3-4.
DOI: [10.1016/S0167-2738\(01\)00844-X](https://doi.org/10.1016/S0167-2738(01)00844-X)
16. Su, D.; Wang, G.; *ACS Nano*, **2013**, 7, 12.
DOI: [10.1021/nm405014d](https://doi.org/10.1021/nm405014d)
17. Sa, N.; Kinnibrugh, T. L.; Wang, H.; Sai Gautam, G.; Chapman, K. W.; Vaughey, J. T.; Key, B.; Fister, T. T.; Freeland, J. W.; Proffit, D. L.; Chupas, P. J.; Ceder, G.; Baren, J. G.; Bloom, I. D.; Burrell, A. K.; *Chem. of Mat.*, **2016**, 28, 9.
DOI: [10.1021/acs.chemmater.6b00026](https://doi.org/10.1021/acs.chemmater.6b00026)
18. Badot, J.-C.; Baffier, N.; *J. of Mat. Chem.*, **1992**, 2, 11.
DOI: [10.1039/JM9920201167](https://doi.org/10.1039/JM9920201167)
19. Clites, M.; Byles, B. W.; Pomerantseva, E. *J. of Mat. Chem. A*; **2016**, 4, 20.
DOI: [10.1039/C6TA02917E](https://doi.org/10.1039/C6TA02917E)
20. Lee, S. H.; DiLeo, R. A.; Marschilok, A. C.; Takeuchi, K. J.; Takeuchi, E. S.; *ECS Electrochem. Letters*, **2014**, 3, 8.
DOI: [10.1149/2.0021408eel](https://doi.org/10.1149/2.0021408eel)
21. Yin, J.; Pelliccione, C. J.; Lee, S. H.; Takeuchi, E. S.; Takeuchi, K. J.; Marschilok, A. C.; *J. Electrochem. Society*, **2016**, 163, 9.
DOI: [10.1149/2.0781609jes](https://doi.org/10.1149/2.0781609jes)
22. Wei, Q.; Jiang, Z.; Tan, S.; Li, Q.; Huang, L.; Yan, M.; Zhou, L.; An, Q.; Mai, L.; *ACS Applied Materials & Interfaces*, **2015**, 7, 33.
DOI: [10.1021/acsami.5b06154](https://doi.org/10.1021/acsami.5b06154)
23. Livage, J.; *Solid State Ionics*, **1996**, 86-88, Part 2.
DOI: [10.1016/0167-2738\(96\)00336-0](https://doi.org/10.1016/0167-2738(96)00336-0)
24. Clites, M.; Pomerantseva, E.; *SPIE Proceedings*, **2016**, 9924.
DOI: [10.1117/12.2238655](https://doi.org/10.1117/12.2238655)
25. Chhowalla, M.; Shin, H. S.; Eda, G.; Li, L.-J.; Loh, K. P.; Zhang, H.; *Nat Chem.*, **2013**, 5, 4.
DOI: [10.1038/nchem.1589](https://doi.org/10.1038/nchem.1589)
26. Naguib, M.; Mochalin, V. N.; Barsoum, M. W.; Gogotsi, Y.; *Adv. Mat.*, **2014**, 26, 7.
DOI: [10.1002/adma.201304138](https://doi.org/10.1002/adma.201304138)



Volume 8, June 2017
Advanced Materials Letters
Editor-in-Chief
Ashutosh Tiwari
Available online at
www.vbripress.com
An Official Journal
IAAM



VBRI Press
Commitment to Excellence

Publish your article in this journal

Advanced Materials Letters is an official international journal of International Association of Advanced Materials (IAAM, www.iaamonline.org) published monthly by VBRI Press AB from Sweden. The journal is intended to provide high-quality peer-review articles in the fascinating field of materials science and technology particularly in the area of structure, synthesis and processing, characterisation, advanced-state properties and applications of materials. All published articles are indexed in various databases and are available download for free. The manuscript management system is completely electronic and has fast and fair peer-review process. The journal includes review article, research article, notes, letter to editor and short communications.

Copyright © 2017 VBRI Press AB, Swedenwww.vbripress.com/aml